A Microcontamination Model For Rotating Disk Chemical Vapor Deposition Reactors

R. W. Davis, E. F. Moore, D. R. Burgess, Jr. and M. R. Zachariah

Chemical Science and Technology Laboratory
National Institute of Standards and Technology
Gaithersburg, MD 20899

This paper presents preliminary results from a model currently under development for gas-phase generated submicron-size contaminant particles (i.e., microcontaminants) in rotating disk chemical vapor deposition reactors. These particles present a problem during semiconductor processing, and this model is intended as a useful tool for gaining a better understanding of this problem. A one-dimensional formulation is employed to model the central section of the reactor, a technique which allows the use of detailed chemical reaction sets. The existing Sandia SPIN code, which contains a solver for the reacting flow, is modified by the addition of an aerosol model for the particles. This model utilizes a moment transport formulation which accounts for convection, diffusion, gravity, thermophoresis, chemical production, coagulation and condensation. Results are presented primarily in terms of reactor performance maps which indicate film growth and contamination rates as functions of substrate temperature. The effects of variations in reactor operating parameters on these maps are discussed.
.

INTRODUCTION

Particle contamination is a major problem afflicting semiconductor processing. The bulk of this problem is now due to gas-phase generated particles as opposed to those particles which may enter with the process stream or flake off equipment surfaces. These gas-phase generated particles are generally small (i.e., submicron) compared with the other types of contaminants and can thus be referred to as "microcontaminants." It is the purpose of the present paper to describe a numerical model currently under development for the formation, growth and transport of microcontaminants in the commonly-used rotating disk chemical vapor deposition (CVD) reactor.

Rotating disk CVD reactors have been the subject of numerous modeling studies involving both nonreacting and reacting flows (1-4), as well as large (> 1μm) contaminant particle transport (5). The interest in this type of reactor stems from several factors. First, the flow is simple and well-characterized when care is taken in the selection of the operating regime. The simple flow patterns lead, in turn, to highly uniform film deposition. Finally, a modified form of the von Karman similarity transformation (1) can be employed to reduce the entire problem to a set of equations solely dependent on the axial coordinate over a large central portion of the reactor. This allows the use of much more detailed chemical reaction sets than would be possible in multidimensions. Using these ideas, a one-dimensional model for the flow and chemistry in the rotating disk reactor has been developed by Sandia National Laboratories and embedded in the SPIN code (6). This code computes velocity, temperature and species distributions, as well as surface deposition rates, in this reactor. The effort to be described here involves the addition of an aerosol model to the SPIN code in order to compute the formation, growth and transport of microcontaminants.

The study of microcontaminants in CVD reactors has been limited due to the great increase in computing resources required by the addition of aerosol dynamics to an already complicated multidimensional chemically reacting flow (7,8). Thus, the one-dimensional nature of the rotating disk formulation makes it an ideal candidate for the inclusion of an aerosol model. The model employed here is similar to that of Whitby and Hoshino (8) which utilized a moment transport formulation in conjunction with a lognormal size distribution function in a two-dimensional horizontal CVD reactor. The lesser dimensionality of the present model, however, allows the use of a much more detailed chemical reaction set.

The results to be presented here are preliminary in nature and serve to illustrate the type of information that will become available from this model during subsequent stages of development, particularly following planned validation experiments. These results will be presented primarily in terms of reactor performance maps which indicate film growth rate and contamination rate as functions of disk temperature. Reactor operating regimes that produce adequate growth rates within acceptable contamination levels

can then be identified. The effects of parameter variations on these maps are assessed as an aid to the optimization of reactor operating conditions.

FLOW/CHEMISTRY SOLUTION

The reactor configuration under consideration here is an infinite radius rotating disk with axial coordinate z. The flow/chemistry solution algorithm is embedded in the SPIN code (6). Transport equations for radial and circumferential momentum, thermal energy and species are of the form

$$\rho\, u\, d\Phi/dz = d/dz\, (\Gamma\, d\Phi/dz) + S_\Phi\,, \qquad (1)$$

where Φ is a general dependent variable, ρ is density, u is axial velocity, Γ is a diffusion coefficient and S_Φ is a source term. State and continuity equations complete the flowfield description. The source terms in the species transport equations are the chemical production rates via gas-phase reactions. These are derived from the law of mass action driven by a user-supplied reaction mechanism. The net flux of chemical species into the substrate results in a film growth rate. Gas-phase and surface chemical kinetics are handled by CHEMKIN (9) and SURFACE CHEMKIN (10), respectively, while the variable transport properties are determined from TRANSPORT (11). While boundary conditions are specified at the disk, there is no specification (at least for the results to be presented here) of the inflow velocity to the reactor. This velocity is allowed to assume a value determined from the natural suction induced by the spinning disk. This ensures a well-behaved flow with very uniform deposition.

AEROSOL MODEL

The aerosol model employed here is a moment transport formulation that accounts for particle formation, growth via condensation and coagulation, and transport via convection, diffusion, gravity and thermophoresis (8,12,13). A lognormal size distribution function is utilized because of its wide applicability in many physical systems (14) and its ease of mathematical manipulation (8,12). The moment transport equation for the present one-dimensional configuration is

$$\rho\, (\, u + c_k\,)\, d\, M_k / dz = d/dz\, (\, \Gamma_k\, d\, M_k / dz\,) + S_k\,, \qquad (2)$$

where c_k is the transport velocity of M_k due to gravity and thermophoresis, Γ_k is the diffusion coefficient of M_k, and S_k is the moment source due to chemical production, coagulation and condensation. The k^{th} moment, M_k, is defined as (14)

$$M_k = 1/\rho \int_0^\infty n(d_p) d_p^{\,k}\, d(d_p)\,, \qquad (3)$$

where d_p is particle diameter. A lognormal number concentration frequency distribution function, n, is employed whereby (12)

$$n = N\, [\, (2\pi)^{1/2} \ln \sigma_g\,]^{-1} \exp\, \{\, -0.5 \ln^2 (d_p/D_{gn}) / \ln^2 \sigma_g\, \}. \qquad (4)$$

Here N is the total number concentration of particles, σ_g is the geometric standard deviation and D_{gn} is the geometric mean size. Equation (2) is solved numerically for k = 0,3,6 which correspond to moments proportional to total number concentration (i.e., N), volume fraction and optical scattering power, respectively (15). All other moments can be determined from these three (8).

The modeling of each term in Eq. (2) is sufficiently complex that it will only be outlined here [see (12) for details]. The moment transport velocity due to gravity is derived by assuming that the gravitational force on a particle is

$$F_g = (\pi\, \rho_p /6)\, d_p^{\,3}\, g\,, \qquad (5)$$

where ρ_p is particle density and g is gravitational acceleration. The thermophoretic moment transport velocity in the free-molecular limit is based on the following force:

$$F_{th} = -P\, \lambda\, d_p^{\,2}\, \nabla T / T\,, \qquad (6)$$

where P is the reactor pressure, λ is the mean free path of the gas molecules and T is temperature. The moment diffusion coefficient, Γ_k , is derived from the following particle diffusion coefficient:

$$D_p = k_B\, T\, (1 + 1.43\, Kn^{1.049}) / (3\pi\mu\, d_p)\,, \qquad (7)$$

where k_B is the Boltzmann constant, Kn is the Knudsen number ($2\lambda / d_p$) and μ is gas viscosity.

The source term, S_k, in Eq. (2) presents the most difficult challenge to model. It consists of three parts:

$$S_k = S_{chem} + S_{coag} + S_{cond}\,, \qquad (8)$$

where the three terms on the RHS represent chemical source, coagulation, and condensation, respectively. The chemical source term, S_{chem}, is the gas-phase formation rate of particle precursors and is an output from the chemical reaction model. The precursors can consist of monomers (single molecules) or clusters of monomers (i-mers) depending on the particular chemical reaction mechanism employed. Once formed, particles grow by means of particle-particle collisions (coagulation) as well as molecular condensation on particle surfaces. The determination of S_{coag} involves the evaluation of complex collision integrals [(8,12,13)] which, for a lognormal distribution, have been approximated by interpolation formulas (16,17). This leads to the following

coagulation source terms:

$$M_0: \; S_{coag} = -4.90\, \rho^2 (k_B T/\rho_p)^{1/2} M_0^{31/16} M_6^{5/48} / M_3^{1/24}, \quad (9)$$

$$M_3: \; S_{coag} = 0, \quad (10)$$

$$M_6: \; S_{coag} = 2.69\, \rho^2 (k_B T/\rho_p)^{1/2} M_0^{5/48} M_3^{13/8} M_6^{13/48}. \quad (11)$$

Note that the volume fraction (~ M_3) does not change as a result of coagulation since particle volumes are conserved during this process.

The condensation source term, S_{cond}, is derived from the following equation for the volume growth rate of a particle (15):

$$dv_p/dt = \alpha P \pi d_p^2 v_m / (2 \pi m k_B T)^{1/2}, \quad (12)$$

where v_p is particle volume, t is time, α and m are sticking coefficient and mass of condensible species molecules (e.g., Si_2H_2) and v_m is molecular volume of the condensed phase (e.g., Si). Note that the condensation source term is of a different nature than the other terms in Eq. (2). This is because evaluation of this term, unlike the others, involves two-way coupling between the chemistry and the aerosol model. Without condensation, the flow/chemistry solution is not dependent on the aerosol solution, since the aerosols in question here are quite dilute. Thus, a single pass through the solution procedure is all that is necessary to obtain the aerosol solution once the flow/chemistry has been determined. When condensation is present, however, the particles act as a sink for gas-phase condensible species and thus affect the chemistry. An iterative procedure, which becomes more difficult as S_{cond} increases, is then required to obtain both the flow/chemistry and aerosol solutions. The importance of condensation depends on the value assigned to the sticking coefficient, α, in Eq. (12), where $0 \# \alpha \# 1$. Since a precise value for this parameter is highly system dependent, as well as a function of particle size and composition, it will be assumed for the purposes of this study that $\alpha = 0.1$. This is large enough to include the effects of condensation in the results without making the computations unduly burdensome.

The solution of the system of equations represented by Eq. (2) is accomplished by means of the LSODE package for the solution of ordinary differential equations (18). The iteration involving this solution coupled with the flow/chemistry solver is carried out on high performance workstations. The boundary conditions are that all moments are zero both at the disk surface and far above it. Particles impact, and thus contaminate, the substrate via a diffusive flux. It is the number and size distribution of this flux which is of primary concern in this modeling effort. In particular, it is of interest to determine the rate at which "killer" particles ($d_p \$ 0.12\mu m$) (19) impact the surface. Reactor operating conditions that maintain this large particle flux within acceptable limits are obviously important to delineate.

CHEMICAL REACTION MECHANISM

The gas-phase chemical reaction mechanism employed in this study consists of reactions involving silicon molecular chemistry that lead to silicon cluster formation (particle nucleation) and subsequent growth. The silicon molecular chemistry is adapted from the reaction set presented in Coltrin et al. (1). A number of reactions have been added to this set in order to adequately describe the chemistry over a range of temperatures and concentrations outside of those considered by these past researchers.

The silicon molecular chemistry can be divided into three general regimes. The first involves the decomposition of silane and the establishment of near steady-state concentrations of silane species, including SiH_4 and Si_2H_6. The second consists of reactions involving silylene species (e.g., SiH_2 and SiH_3SiH) and hydrogen elimination to form small silicon molecules. Finally, the third general regime consists of reactions involving these small silicon molecules and/or molecular clusters, including Si_2H_2, Si_2, Si and Si_3.

The reaction set describing silicon cluster formation essentially consists of enumerating all the possible combinations. Small clusters react to form larger and larger clusters which eventually become particle nucleation sources. Silicon hydride, Si_2H_2, is used as the condensible species.

RESULTS AND DISCUSSION

The baseline configuration employed for the initial tests of the microcontamination model consists of an atmospheric pressure reactor with a disk rotation rate of 1000 rpm and argon diluent containing 0.1% mole fraction of silane. The inlet flow velocity of approximately 3.35 cm/s is naturally induced by the disk rotation, and all inlet boundary conditions are applied at z = 2 cm. The effects of variations from the baseline conditions are presented by means of reactor performance maps over a disk temperature range of 1000 K to 1400 K, which is typical for silicon epitaxy (3).

Figure 1 depicts the total number concentration (M_0) and average particle size (M_1/M_0) as functions of height above the disk for the baseline case at disk temperatures of 1100 K and 1400 K. Both of these quantities are seen to reach their maximum values inside the thermal boundary layer just above the disk. While the average particle size is not a strong function of temperature, the total number concentration increases with temperature. As will be shown, this is reflected in greater substrate contamination levels at higher temperatures. The decrease in average particle size approaching the substrate is due to the fact that diffusion is the primary mechanism of particle transport toward the surface, and the diffusion coefficient, Eq. (7), varies inversely with d_p or d_p^2 depending on size (14). This inverse dependence of the diffusion coefficient on particle size is fortuitous in that it acts to reduce substrate contamination by

large particles. Total number concentrations, M_0, near the surface are reduced due to the thermophoretic component of c_k which is independent of particle size (12,14).

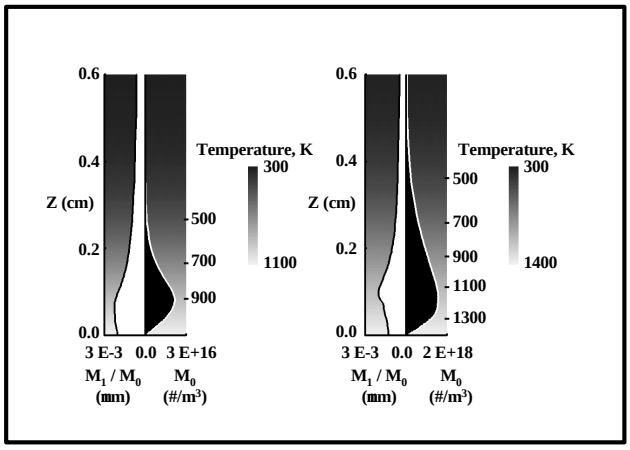

FIGURE 1. Total number concentration (M_0) and average particle size (M_1/M_0) with a thermal contour background for the baseline case with disk temperatures of 1100 K and 1400 K.

As noted previously, reactor performance maps are the primary output from this model. The performance map for the baseline case is presented in Fig. 2 as the solid plots. These two plots represent the temperature dependence of the surface film growth rate in μm / minute and the large "killer" particle surface contamination rate per m^2 per time required to deposit one μm of film thickness. This adjustment of the contamination rate to reflect variations in film growth rate provides a means of assessing the severity of the contamination problem independent of how much fabrication time is necessary. Values of the contamination rate above the horizontal axis (i.e., >10) would probably be considered unacceptable (19). However, it is noted that trends here are more reliable than absolute values since these results can be highly sensitive to modeling assumptions (such as sticking coefficient) that have yet to be experimentally validated. It can be seen from Fig. 2 that the surface growth rate peaks at about 1100 K and then decreases with temperature as the contamination rate rapidly rises. This drop in film growth rate is due to the presence of increasing numbers of gas-phase contaminant particles which act as an added surface for silicon deposition. This increase in gas-phase particles with temperature (along with a broad size distribution) also leads to the increasing surface contamination rate. Thus, it can be seen from the solid plots in Fig. 2 that the optimum disk temperature for the baseline case is approximately 1100 K.

The effects of variations in the reactor operating conditions from the baseline case will now be assessed. A set of plots (dashed lines) in Fig. 2 illustrates the difference between the baseline pressure of 1 atm and a reduced pressure of 0.1 atm. As can be seen, lowering the pressure results in both lower film growth rate and lower surface contamination, which are at least partially attributable to decreased reaction rates at the lower pressure. Therefore, if

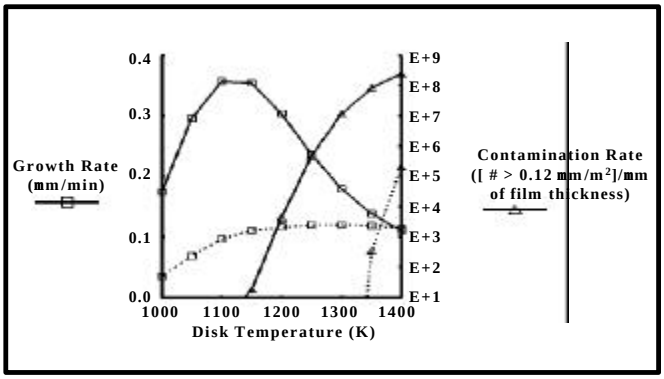

FIGURE 2. Reactor performance map for the baseline case and effect of pressure reduction (—— 1.0 atm; ------- 0.1 atm).

slower growth rates are acceptable, decreasing the reactor pressure is an effective method of contamination control. The effect of varying the disk rotation rate from 500 rpm to 1500 rpm is presented in Fig. 3. It is clear from this figure that increasing the rotation rate results in an increased film growth rate along with moderately decreased surface contamination. It is noted, however, that too large a disk rotation rate can result in undesirable recirculation zones adjacent to the walls in an actual reactor configuration (20). Finally, changes in performance due to increasing the inlet silane concentration from a mole fraction of 0.1% to 0.3% are depicted in Fig. 4. The growth rate, as expected, increases as does the contamination rate (albeit slightly) over most of the temperature regime. At high temperatures, however, increasing the silane concentration has almost no effect on both the growth and contamination rates. This is because the increased silane concentration is depleted at the high temperatures due to increased condensation on gas-phase particles. This reduces surface growth rate and results in larger particles which less readily diffuse to the substrate.

CONCLUDING REMARKS

Preliminary results have been presented from a microcontamination model for rotating disk CVD reactors which is currently under development. The model utilizes a one-dimensional formulation to model the cylindrical central section of the reactor. This reduction in dimensionality allows the use of detailed chemical reaction sets. Reactor performance maps have been presented that demonstrate decreased large-particle contamination rates with reduced pressure and increased disk rotation rate. It has also been noted that thermophoresis and a size-dependent particle diffusion coefficient act to ameliorate substrate contamination. Finally, because of the complexity of this model, the only method of quantitatively verifying the results is through comparisons with experimental data, an effort that is currently underway. An experimentally-validated microcontamination model should prove to be a powerful tool for both the design and operation of rotating disk reactors.

REFERENCES

1. Coltrin, M. E., Kee, R. J. and Evans, G. H., *J. Electrochem. Soc.* **136**, no. 3, 819-829 (1989).
2. Breiland, W. G. and Evans, G. H., *J. Electrochem. Soc.* **138**, no. 6, 1806-1816 (1991).
3. Jensen, K. F. and Einset, E. O., *Ann. Rev. Fluid Mech.* **23**, 197-232 (1991).
4. Ho, P., Coltrin, M. E. and Breiland, W. G., *J. Phys. Chem.* **98**, no. 40, 10138-10147 (1994).
5. Davis, R. W., Moore, E. F. and Zachariah, M. R., *J. Crystal Growth* **132**, 513-522 (1993).
6. Coltrin, M. E., Kee, R. J., Evans, G. H., Meeks, E., Rupley, F. M. and Grcar, J. F., "SPIN (Version 3.83): A FORTRAN Program for Modeling One-Dimensional Rotating - Disk/Stagnation-Flow Chemical Vapor Deposition Reactors," Sandia National Laboratories Report SAND91-8003, 1991.
7. Okuyama, K., Huang, D., Seinfeld, J. H., Tani, N. and Kousaka, Y., *Chem. Eng. Sci.* **46**, no. 7, 1545-1560 (1991).
8. Whitby, E. and Hoshino, M., *J. Electrochem. Soc.* **143**, no. 10, 3397-3404 (1996).
9. Kee, R. J., Rupley, F.M. and Miller, J. A., "CHEMKIN II: A FORTRAN Chemical Kinetics Package for the Analysis of Gas Phase Chemical Kinetics," Sandia National Laboratories Report SAND89-8009, 1989.
10. Coltrin, M. E., Kee, R. J. and Rupley, F. M., "SURFACE CHEMKIN (Version 4.0): A FORTRAN Package for Analyzing Heterogenous Chemical Kinetics at a Solid-Surface-Gas-Phase Interface," Sandia National Laboratories Report SAND90-8003B, 1991.
11. Kee, R. J., Dixon-Lewis, G., Warnatz, J., Coltrin, M. E. and Miller, J. A., "A Fortran Computer Code Package for the Evaluation of Gas-Phase Multicomponent Transport Properties," Sandia National Laboratories Report SAND86-8246, 1986.
12. Whitby, E. R., McMurry, P. H., Shankar, U. and Binkowski, F. S., "Modal Aerosol Dynamics Modeling," U.S. Environmental Protection Agency Report for Contract No. 68-01-7365, 1991.
13. Whitby, E. R. and McMurry, P. H., *Aerosol Sci and Tech.* **27**, No. 6, 673-688 (1997).
14. Hinds, W. C., *Aerosol Technology*, New York: John Wiley, 1982.
15. Friedlander, S. K., *Smoke, Dust and Haze*, New York: John Wiley, 1977.
16. Dobbins, R. S. and Mulholland, G. W., *Comb. Sci. And Tech.* **40**, 175-191 (1984).
17. Zachariah, M. R. and Semerjian, H. G., *AIChE Journal* **35**, no. 12, 2003-2012 (1989).
18. Radhakrishnan, K. and Hindmarsh, A. C., "Description and Use of LSODE, the Livermore Solver for Ordinary Differential Equations," Lawrence Livermore National Laboratory Report UCRL-ID-113855 (NASA Reference Publication 1327), 1993.
19. "The National Technology Roadmap for Semiconductors," Semiconductor Industry Association, 1994.
20. Biber, C. R., Wang, C. A. and Motakef, S., *J. Crystal Growth* **123**, 545-554 (1992).

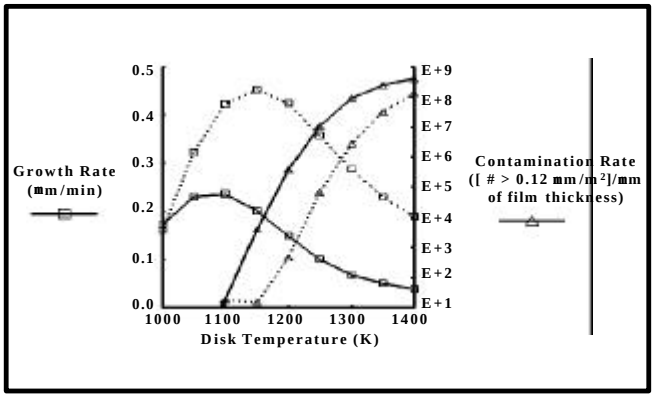

FIGURE 3. Effect of disk rotation rate on the reactor performance map (—— 500 rpm; ------- 1500 rpm).

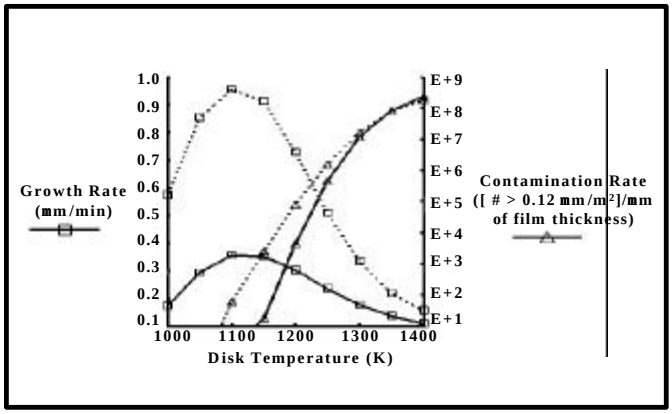

FIGURE 4. Effect of inlet silane mole fraction concentration on the reactor performance map (—— 0.1%; ------- 0.3%).